



Deep-learning-enhanced digital twinning of complex composite structures and real-time mechanical interaction

Xiaoyao Xu, Guowen Wang, Han Yan, Laibin Zhang, Xuefeng Yao *

Department of Engineering Mechanics, Applied Mechanics Lab, Tsinghua University, Beijing, 100084, PR China



ARTICLE INFO

Handling Editor: Prof. Y.-W. Mai

Keywords:

Digital twin
Machine learning
Fabric rubber composites
Anisotropy
Mechanical properties

ABSTRACT

Digital twins are undergoing growth that enables highly informative and scaleable interaction between physical objects and virtual twins, which is of great significance to the life cycle analysis of composites. Real-time fine evolution is challenging due to vast combinations of input features and high-resolution calculated variables. Here, we systematically demonstrate an AI-based methodology for digital twinning of complex composite structures. First, three types of deep neural networks are created with optionally used autoencoders as surrogate models, with architectures and data processing inspired by the rule-of-mixture of composites. Second, the prediction accuracy and efficiency are evaluated quantitatively and qualitatively, demonstrating the feasibility of predicting 3D displacement and stress fields directly from sensing data of temperature, pressure and loading displacement, and the optimal architecture is selected to be the evolving digital twin. Finally, the real-time interactive experiments are relayed to the digital twin and demonstrated that it can interact with physical objects and evolve online with high accuracy. These results indicate that the computational time can be reduced by 3~6 orders of magnitude with high information intensity and scalability compared with conventional numerical and experimental methods, which opens up the avenues for the cost-effective and efficient development of digital twin services for composites.

1. Introduction

High-performance composites with complex structure reinforced skeletons are increasingly applied to aerospace components, engineering biomaterials, wearable computing and energy harvesting due to excellent mechanical properties and versatility [1–3]. As indispensable smart technologies of the advancement for Industry 4.0 initiatives and smart manufacturing [4], digital twins have been used to complex systems of different scales which is extensively regarded as a paradigm shift [5–7]. The integration of advanced information technologies and the design and evaluation of composites is expected to reduce the high computing cycles and promote composite digital twins for effectively identifying physical status and extending new capabilities in engineering applications.

The digital twin is characterized by two advantageous features [8]: (i) high-fidelity virtual representations and (ii) real-time updates with the changing of their physical counterparts. Recently, advances in computational science have sparked interests in realizing digital twins in fields as diverse as aerospace, manufacturing, earth-system science and power engineering [3,9–14]. For complex composites with accurate

analysis requirements, as a trade-off, their digital twin studies place emphasis on structural health management by means of specific indicators, such as crack propagation length [15], cavity formation [16] and weld penetration depth [17]. However, physical fields such as stress and strain distributions are the hallmark of the mechanics among refined computing requirements, which is essential to many design applications and engineering analyses. The physics-based simulation methods have long been used to drive composites design and discovery over the past few decades [18–20]. It is intractable to realize high-fidelity real-time computations at affordable expense due to the contradiction between the scale of solution and the computing performance [9,21]. Notably, digital twin frameworks used across industries have yet to fully incorporate predicted physical fields or directly link material characteristics to service environments. Hence, to gain more insights into the digital twin, it is crucial to develop further models.

At the same time, most machine learning approaches have promptly evolved into deep learning to predict the constitutive relationships of materials in recent years [22–25]. Meaningful progress has been made in the forecast of strain and stress fields for composites [26–29], suggesting

* Corresponding author.

E-mail address: yxf@mail.tsinghua.edu.cn (X. Yao).

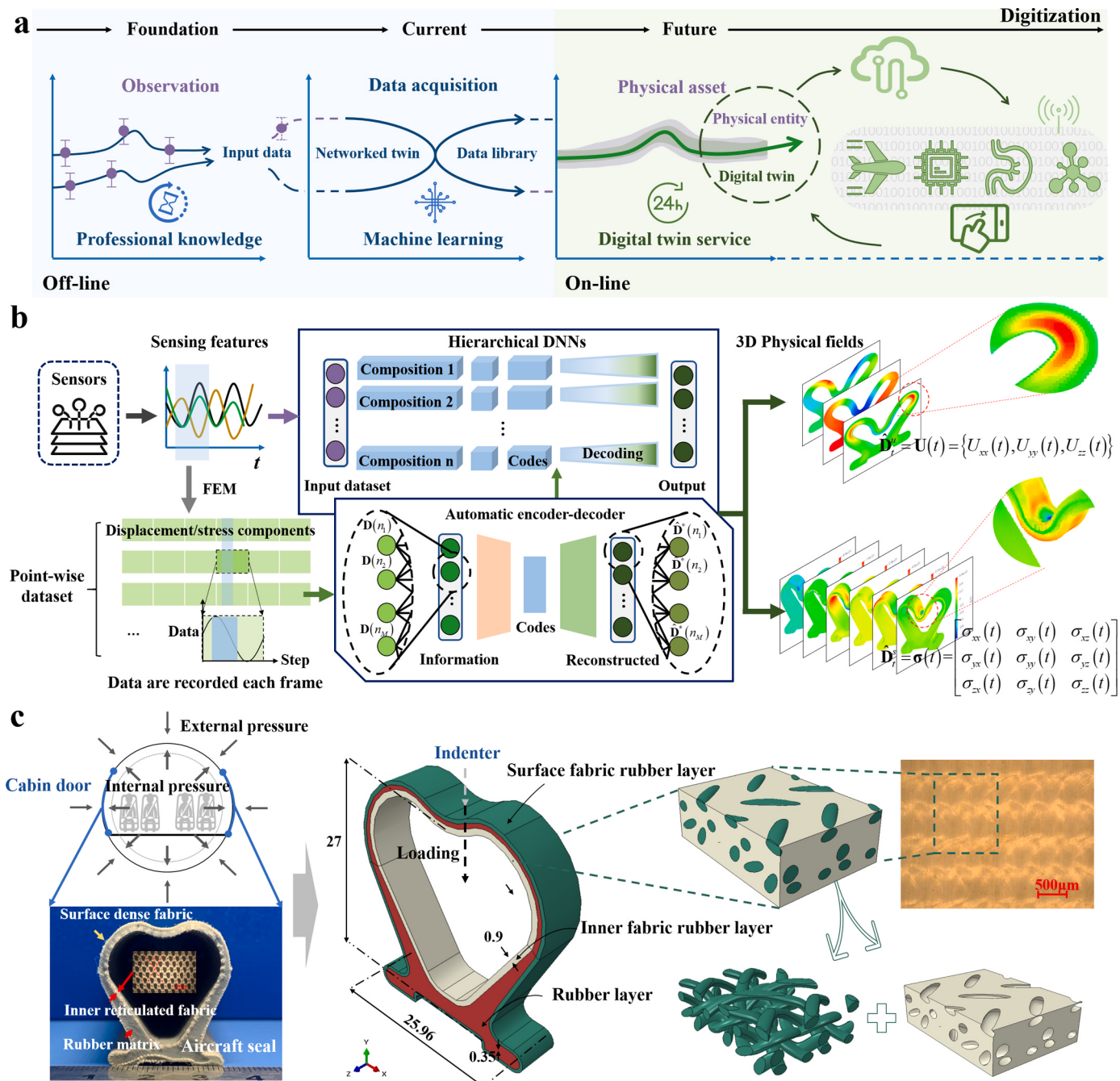


Fig. 1. Schematics of the digital twin and physics involved in the representative complex composite: (a) The conceptual diagram of the digital twin and its potential applications. The top and down notes focus on changes of physical entities and digital solutions, respectively. (b) Digital twin workflows based on deep learning, including layered architectures and decoders for composite components, where the insets show results from sensing features of temperature, pressure and loading displacement to three-dimensional full-field displacement and stress information. (c) Schematic diagram of representative complex fabric rubber composite used in aviation, its meso-structures and macro- and mesoscopic analysis method.

the possibility of integrating the digital twin and resolving its limitations. However, most machine learning assisted mechanical approaches focus on specific indicators and characteristic information or only applied to discrete scenes. Besides, existing results showed that color images of composites are mostly used as input data carrying geometric, boundary and RGB information, so distinctive neural networks such as convolutional neural networks (CNNs) and segmentation-based U-Net can be used for prediction. Furthermore, for several scenarios like aerospace, installing additional image sensors and performing additional tests are invasive, high investment, high design complexity and energy-wasting. Therefore, a computational strategy is required for

realizing real-time synergies between mechanical and decision models in such time-sensitive scenarios and limited IT infrastructure. In light of the current state of the art, the potential of integration between deep learning and digital twins remains in its infancy.

In this study, a framework of digital twin is presented for complex composite structures (CCSs) and its full-field predictive and interactive feasibility are demonstrated in conjunction with machine learning methods. The hierarchical deep neural networks (H-DNNs) architecture inspired by multicomponent and rule-of-mixture of composites [30] is developed for digital twins. In contrast to image-dependent deep learning image processing algorithms, H-DNNs predict

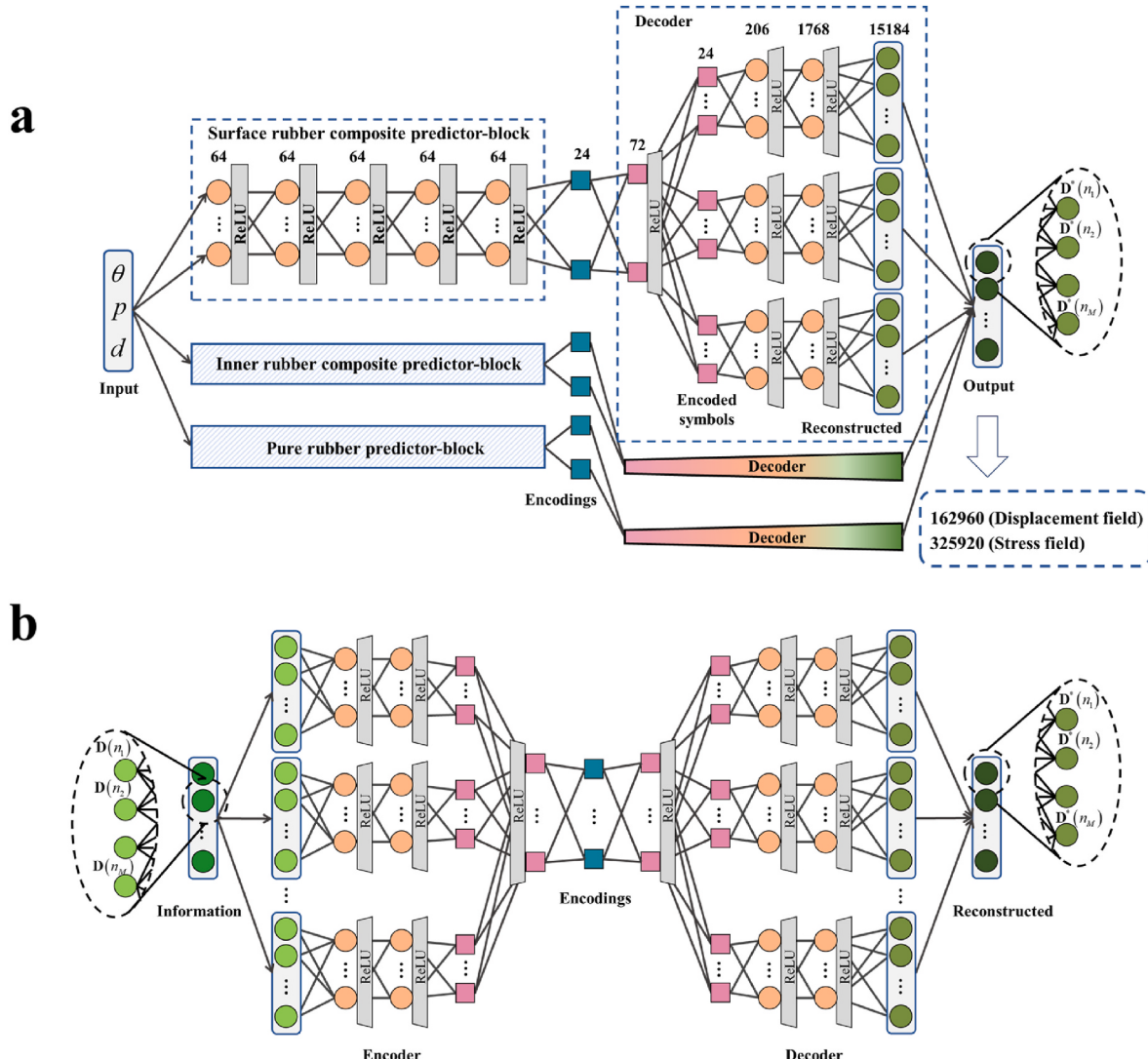


Fig. 2. Frameworks of the H-DNNs predictor and automatic encoder-decoders: (a) Architecture of the hierarchical deep neural networks based on autoencoders for three-dimensional field components. The corresponding network parameters of surface fabric rubber are marked. (b) Architecture of the automatic encoder-decoder for three-dimensional field components.

three-dimensional integral mechanical information of CCS directly from the succinct sensing data for timing-sensitive physical analysis and design. The real-time interactive experiments are relayed to the digital twin, and quantitative and qualitative performance test results demonstrate the accuracy and efficiency of the proposed method.

2. Materials and methods

2.1. Framework of the digital twin

The general framework of a digital twin that integrates the macro- and mesoscopic characteristics of composites with deep-learning technology for predicting mechanical information in real time is presented in Fig. 1a; its depictions can be divided into offline and online phases in chronological order, including three important modules: (i) the physical system, (ii) twin data and (iii) the digital twin. First, as the foundation of creating a digital twin, simulation-observation fusion and verification are essential to ensure the accuracy and validity of digitally created objects, which further allows the generation of learning datasets from computational models. Second, before defining a digital twin state, the information sufficient to support the practical usage must be considered, including performance evaluation, selection of representative

characteristics and model fidelity. The optimal machine learning approach is selected to create a constantly updated digital twin. Furthermore, the physical entities are equipped with data acquisition software and hardware, which can transmit system data to the digital twin in real time. Finally, the deep learning-based digital twin will co-evolve with the physical entity and merge the virtual world with the real world in the service phase.

2.2. Computational models comprising the CCS digital twin

As shown in Fig. 1b, the H-DNN architecture encapsulates the prediction flow of 3D physical fields for CCS, which are divided into two modules: predictor and autoencoder. Considering that the properties of composite materials are affected by environmental parameters, loadings such as pressure and displacement are usually measurable, and the influence of complex boundary conditions can be implicitly described by the hyperparameters of the neural network, so compared with previous image-dependent studies, the sensing data, as the only inputs, are selected to succinctly represent the evolution of material properties and boundary conditions of the complex composites over time, and the full-field mechanical information is predicted directly by the predictor. Dimensionality reduction is a major step towards solving complicated

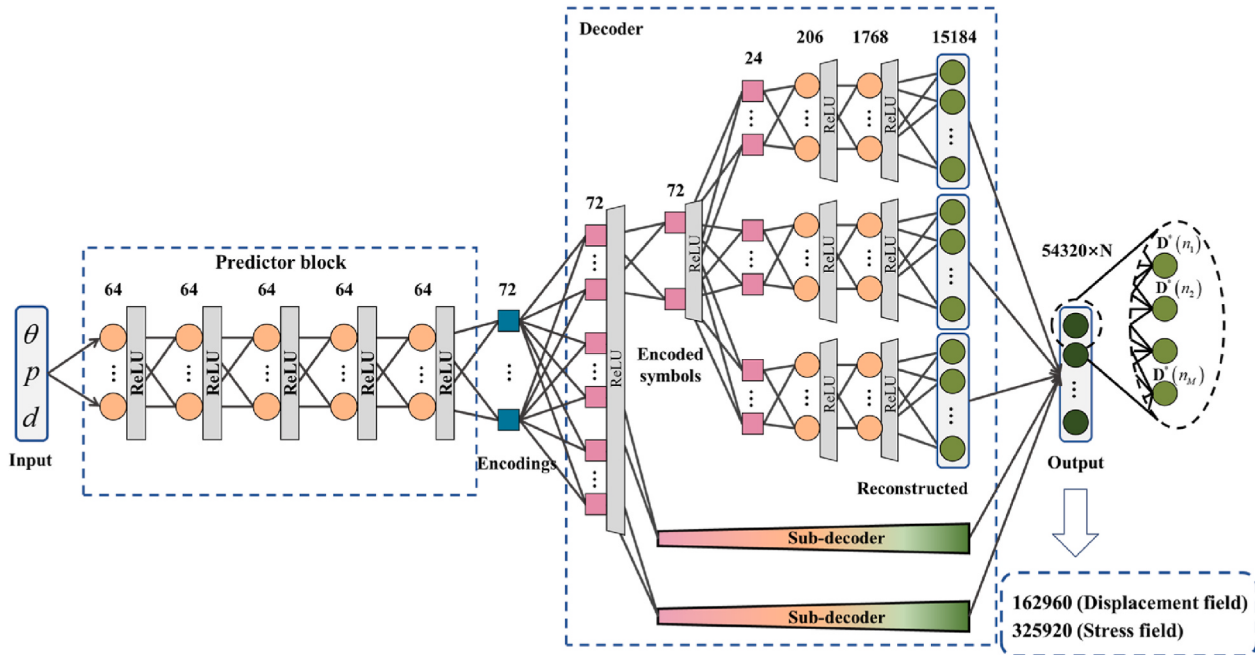
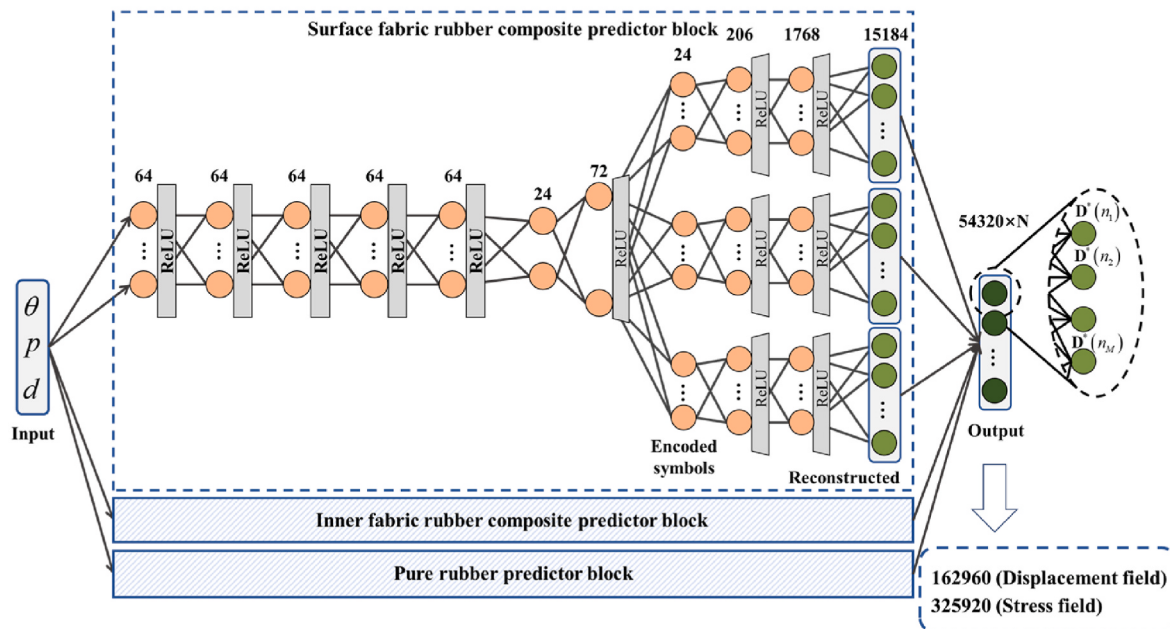
a**b**

Fig. 3. Frameworks of the U-DNNs and D-DNNs predictors: (a) Architecture of the unified deep neural networks based on autoencoders for three-dimensional field components. (b) Architecture of the hierarchical direct deep neural networks without autoencoders for three-dimensional field components. The corresponding network parameters of surface fabric rubber are marked.

procedures with high-dimensional datasets involved in 3D composites, so the automatic encoder-decoders (as the trapezoidal gradient box shown in Fig. 1b) are trained to capture the intrinsically low-dimensional structure of datasets correlated with the output results for training [31]. Then H-DNNs with decoding module (as the upper first box shown in Fig. 1b) are designed as the predictor $\zeta(\cdot)$ that first map input features into encodings, then the decoding module converts these encodings into desirable outputs $\hat{\mathbf{D}} = \zeta(\mathbf{x}, \chi)$. The rule-of-mixture [30] is widely used in composite engineering to calculate the weighted contributions of different components. Here, the contributions of different composite components are individually considered; that is, the same number of prediction and autoencoder blocks according to the composite components is used in the H-DNNs.

To explore the effects of dimensionality reduction of data and

hierarchical training on the learning accuracy and efficiency of CCS digital twins, three neural networks with different architectures are designed as surrogate models of physical fields, proving that H-DNNs work well: (i) H-DNNs, (ii) unified deep neural networks based on autoencoders (U-DNNs) and (iii) direct deep neural networks (D-DNNs). It should be noted that the larger the dimension of the deep learning dataset, the more severely the sensitivity of the input attributes to the output results will be tested. For assessing the significance of the autoencoder, the best performance of the D-DNNs is selected to be compared with H-DNNs and U-DNNs, that is, the D-DNNs is also designed as hierarchical training architectures. Moreover, it is obvious that the displacement field and the stress field have different physical meanings, so they are also trained individually based on independent architectures, in which the number and layers of neurons are adjusted according to computational accuracy and efficiency. The H-DNN

architecture is given with the explanation of the parameters of the architecture for predicting the stress in the next section for concise elaboration.

2.2.1. Hierarchical DNNs model based on autoencoders

As illustrated in Fig. 2, the architecture and data flow of the H-DNNs integrate two modules: predictor and autoencoder. Setting $\mathbf{x} = (\mathbf{x}_0, \dots, \mathbf{x}_n)^T \in \mathbb{R}^{n \times m}$ as input data with feature dimensionality m and sample scale n , the output data $\hat{\mathbf{D}} = \zeta(\mathbf{x}; \chi)$ can be obtained by the nonlinear relationship between the input data and output scores. Noting that the $\chi = \{\mathbf{w}, \mathbf{b}\}$ is used to estimate the values of neurons and optimize for minimizing the loss function. The nonlinear mapping relationship from constitutive parameters and boundary conditions to 3D displacement and stress fields of complex fabric rubber composite can be expressed as:

$$\hat{\mathbf{D}}_t^k = \zeta^k \left(\underbrace{\alpha_i, \beta_i, \dots}_{\text{constitutive}}; \underbrace{p_i, d}_{\text{boundary}} ; \chi \right) = \zeta^k(\theta(t), p_i(t), d(t); \chi) \quad (1)$$

where the superscript k equals d and s for the displacement and stress field, respectively. $\zeta^k(\cdot)$ represents the H-DNNs for the displacement and stress field. α_i, β_i, \dots represent the constitutive parameters of different composite components. p_i represents the external and internal pressure conditions applied to the fabric rubber composite. Here, the subscript i represents the number of parameters with similar physical meaning. d represent the displacement loading condition. Here, t represents the current time, which means taking the field components from the present configuration. As mentioned above, the constitutive parameters change with temperature, so temperature, pressure, and compression are functions of time in practice. For 3D problems, the output displacement field $\hat{\mathbf{D}}_t^u$ and stress tensor $\hat{\mathbf{D}}_t^s$ are expressed as:

$$\hat{\mathbf{D}}_t^u = \mathbf{U}(t) = \{U_{xx}(t), U_{yy}(t), U_{zz}(t)\} \quad (2)$$

$$\hat{\mathbf{D}}_t^s = \boldsymbol{\sigma}(t) = \begin{bmatrix} \sigma_{xx}(t) & \sigma_{xy}(t) & \sigma_{xz}(t) \\ \sigma_{yx}(t) & \sigma_{yy}(t) & \sigma_{yz}(t) \\ \sigma_{zx}(t) & \sigma_{zy}(t) & \sigma_{zz}(t) \end{bmatrix} \quad (3)$$

The back-propagation algorithm is used to calculate the change in the loss function. In combination with the displacement field and strain field in Eqs. (2) and (3), the explicit expression of the backwards propagation equation can be obtained based on the chain rule [32]. As shown in Fig. 2a, the different physical components (displacement and stress) of different composites (surface fabric rubber, inner fabric rubber and pure rubber) are calculated by independent neural network blocks and decoders. For example, the field components of different composites are encoded into 24 encodings, and the total number of encodings is the sum of three composite layers, which is 72. The encoding-decoding procedures are implemented by a bidirectional autoencoder, as shown in Fig. 2b.

2.2.2. Unified DNNs models based on autoencoders

Compared with the architecture and data flow of H-DNNs model, the U-DNNs model trains the data of surface fabric rubber composite layer, inner fabric rubber composite layer and pure rubber layer in unified networks, as shown in Fig. 3a. The difference between H-DNNs model and U-DNNs model is that the autoencoder encodes the overall field components of complex fabric rubber composite into 72 encodings. As

mentioned above, the independent autoencoder and neural network are used for displacement field and stress field, and the number of neurons per layer in the networks is seen in Fig. 3a.

2.2.3. Direct DNNs models

D-DNNs consists of multiple separate networks for prediction with similar architectures to autoencoders, which is designed to predict the displacement and stress fields of complex fabric rubber composite. That is, to facilitate comparison with H-DNN and U-DNN, the network architecture and parameters of D-DNN are as consistent as possible with those of H-DNN and U-DNN using autoencoders and the expected optimal multi-layer separate network is used. However, no autoencoder is used and no decoding process is performed in D-DNN. Fig. 3b shows the architecture of D-DNNs model for the displacement field with ten hidden layers, and the controlled architecture parameters for stress field are also noted.

In general, H-DNN uses both the hierarchical architecture and autoencoder; U-DNN uses a unified architecture and autoencoder; D-DNN uses the hierarchical architecture like H-DNN, but without the autoencoder.

2.3. Material and manufacturing involved in the CCS entity

In this study, we focus on the major issues of realizing the digital twin and provide specific examples from the intelligent composite application. Fig. 1c shows the fabric rubber composite with complex internal structures and irregular shapes. As shown on the right of Fig. 1c, the complex fabric rubber composite is adopted as airtight sealing components in the aerospace field and subjected to ambient temperature, external pressure, internal (cabin) pressure and loading by fuselages' structure when acting as a cabin door seal. The failure of the sealing structure for the aircraft door may lead to the rapid pressure release of the aircraft cabin in the cruising state, which directly affects the flight safety. Although large-scale computational simulations exist, they are often too slow to be used in the fast-paced and mobile computing of the field in the cruising environment. Therefore, there is a growing demand for real-time monitoring of the operation status for the composite seal structure, so the complex fabric rubber composite is selected as typically time-sensitive and decision-making scenario for digital twins of CCS.

Macro- and mesoscopic approaches were indicated as an effective method to model the mechanical behaviours of this complex composite in our previous work [33,34]. As shown in Fig. 1c and Supplementary Fig. 1, the complex composite can be divided into pure rubber, surface dense fabric rubber and inner reticulated fabric rubber layers, which are characterized by anisotropic hyperelastic models. Considering the material properties at different temperatures, the temperature variable θ can be introduced into the Mooney-Rivlin model [35,36] to describe the mechanical behavior of rubber, and the strain energy function can be expressed as:

$$W_R = C_{10}(\theta)(I_1 - 3) + C_{01}(\theta)(I_2 - 3) + \frac{1}{Z_1(\theta)}(J - 1)^2 \quad (4)$$

where $C_{10}(\theta)$ and $C_{01}(\theta)$ are the constitutive constants of rubber, which could be determined by experiments. $Z_1(\theta)$ and J describe the compressive behaviors. I_1 and I_2 are invariants of the right Cauchy-Green deformation tensor \mathbf{C} .

The constitutive model of the inner fabric rubber composite considering temperature changes can be expressed as [37,38]:

$$W_{dev} = W_{matrix} + W_{fiber} + W_{interaction} = C_{10}(\theta)(I_1 - 3) + C_{01}(\theta)(I_2 - 3) + \frac{k_1(\theta)}{2k_2(\theta)} \sum_{j=4,6} \left[e^{k_2(\theta)(\max(j, 1) - 1)^2} + \frac{k_2(\theta)}{4}(\max(I_j, 1) - 1)^2 - 1 \right] + \frac{k_3(\theta)}{k_4(\theta)}(I_1 - 3)e^{k_4(\theta) \left(\sum_{j=4,6} I_j - 2 \right)} \quad (5)$$

where the first term could be derived from the constitutive model of pure rubber. k_1 and k_3 are stress-like material parameters with the unit of MPa, and stiffness increasing rates k_2 and k_4 are dimensionless material parameters. I_4 and I_6 are pseudo-invariants described by the orientation tensors of the inner mesh fabric.

The mechanical model of dense surface fabric rubber is difficult to be analytically established. According to the mesoscopic modelling method, the engineering constants of anisotropic constitutive relationship is applied to characterize surface fabric rubber composite [33]:

$$\bar{\varepsilon}_{ij} = S_{ijkl}(\theta) \bar{\sigma}_{ij} \quad (6)$$

where $S_{ijkl}(\theta)$ is the equivalent elastic tensor of the representative volume element of surface fabric rubber composite, and it could be expressed as:

$$S_{ijkl}(\theta) = \begin{bmatrix} 1/E_x(\theta) & -\nu_{yx}(\theta)/E_y(\theta) & -\nu_{zx}(\theta)/E_z(\theta) & 0 & 0 & 0 \\ -\nu_{xy}(\theta)/E_x(\theta) & 1/E_y(\theta) & -\nu_{zy}(\theta)/E_z(\theta) & 0 & 0 & 0 \\ -\nu_{xz}(\theta)/E_x(\theta) & -\nu_{yz}(\theta)/E_y(\theta) & 1/E_z(\theta) & 0 & 0 & 0 \\ 0 & 0 & 0 & 1/G_{xy}(\theta) & 0 & 0 \\ 0 & 0 & 0 & 0 & 1/G_{yz}(\theta) & 0 \\ 0 & 0 & 0 & 0 & 0 & 1/G_{zx}(\theta) \end{bmatrix} \quad (7)$$

where $\bar{\sigma}_{ij}$ and $\bar{\varepsilon}_{ij}$ are the average stress and average strain of the representative volume element, which can be obtained by averaging the stress and strain of elements in the representative volume element. The index ij indicates the acting direction of the average stress or the measuring direction of the average strain. These constitutive parameters were tested and listed in Tables S5–S7.

The relationship of rule-of-mixture may be mainly reflected in hierarchical network design and data homogenization of repeated nodes predicted from hierarchical networks. After H-DNN gives the predicted results of physical field components, the output of multiple separate networks is post-processed by referring to the idea of mixing rules, that is, the homogenization is carried out in a way that considers the relative proportion of the predicted results of each separate network. The surface fabric rubber layer, the rubber layer and the inner fabric rubber layer are predicted by separate networks, and the predicted results contain overlapping nodes, which are homogenized by the weight of the number of overlapping nodes. In this study, the mean value of repeated node results was taken as the final output.

2.4. Generation of FEM dataset and pretreatment

The identical virtual state under the same environmental and structural boundary conditions as the aircraft is established based on the finite element methods (FEM) to obtain the real field information. The selection of representative features can be related to the ease of operation, sensing, integration, and interpretation of reduced-order models [39]. In order to realize the real-time physical fields of complex fabric rubber composites under different service environments during flight, the full-field deformation and stress are selected as output features. As mentioned in Section 2.2, the input signal depends on the actual environment in which the physical entity is affected and should be easy to integrate, stable to test and energy efficient. For example, the

temperature θ , external pressure P_{ext} , internal pressure P_{int} and loading displacement d affect the mechanical response of the CCS and can be obtained directly from the aircraft's integrated sensors, which are reliable in critical but image-inaccessible areas such as aircraft slits or in harsh operating conditions with poor transmission and are hence chosen as input features. It is noted that d represents that the CCS is loaded vertically in its center by the indenter of the same size as the fuselage structure (see Fig. 1c). In practice, cabin pressure in practice is usually maintained due to pressurization, so the temperature, external pressure and load displacement are 3 inputs to the surrogate models. Table S8 lists the value ranges of inputs.

Noting that for more complex digital twins, the number of sensors required may be much greater. The case in Section 3.1.2 shows an example of verifying the overall compression performance with an additional force sensor, which is used to represent one of the potential

applications of additional sensors.

The temperature-dependent constitutive parameters in FEM are mapped to the temperature input; the pressure sensor corresponds to external pressure and cabin pressure on the composites, and the displacement sensor corresponds to the loading displacement of indenter, which are the pressure loading and displacement loading parameters of FEM, respectively. Taking the computational efficiency-cost problem and convergence into consideration, the design of experimental methodology [40] is adopted to generate training sets based on the FEM model containing 38342 elements. The surface fabric rubber composite, inner fabric rubber composite and pure rubber layer have 15184, 13120 and 26016 nodes, respectively. There are 45330 non-repeating nodes in the CCS, and the vector lengths of the displacement field and stress field are 135990 and 271980, respectively. The 3D displacement and stress fields under working conditions are collected, and all node coordinates in the data set are sorted by node number to directly form high-dimensional vectors in datasets. The geometry of the part is implicitly embedded into the autoencoder. Such data relationship between rows suggests the use of DNNs. Noting that the selective use of CNN could be referred to the work of [29] to process the dataset according to a specified rule for the convolution calculation of the middle layers and autoencoder, accompanied by a reserved input layer. A total of 294 samples within the value ranges of the input features were computer-generated, representing all possible conditions in the design space. More ways to select sample sizes can be seen in related works [13, 14] and in conjunction with the data enhancement method.

2.5. Evaluation methods

These three DNNs architectures are implemented in TensorFlow as surrogate models, detailed network parameters can be obtained in Tables S1–S4. Once the autoencoders are determined by unsupervised learning, the parameters of the nonlinear mapping module are obtained

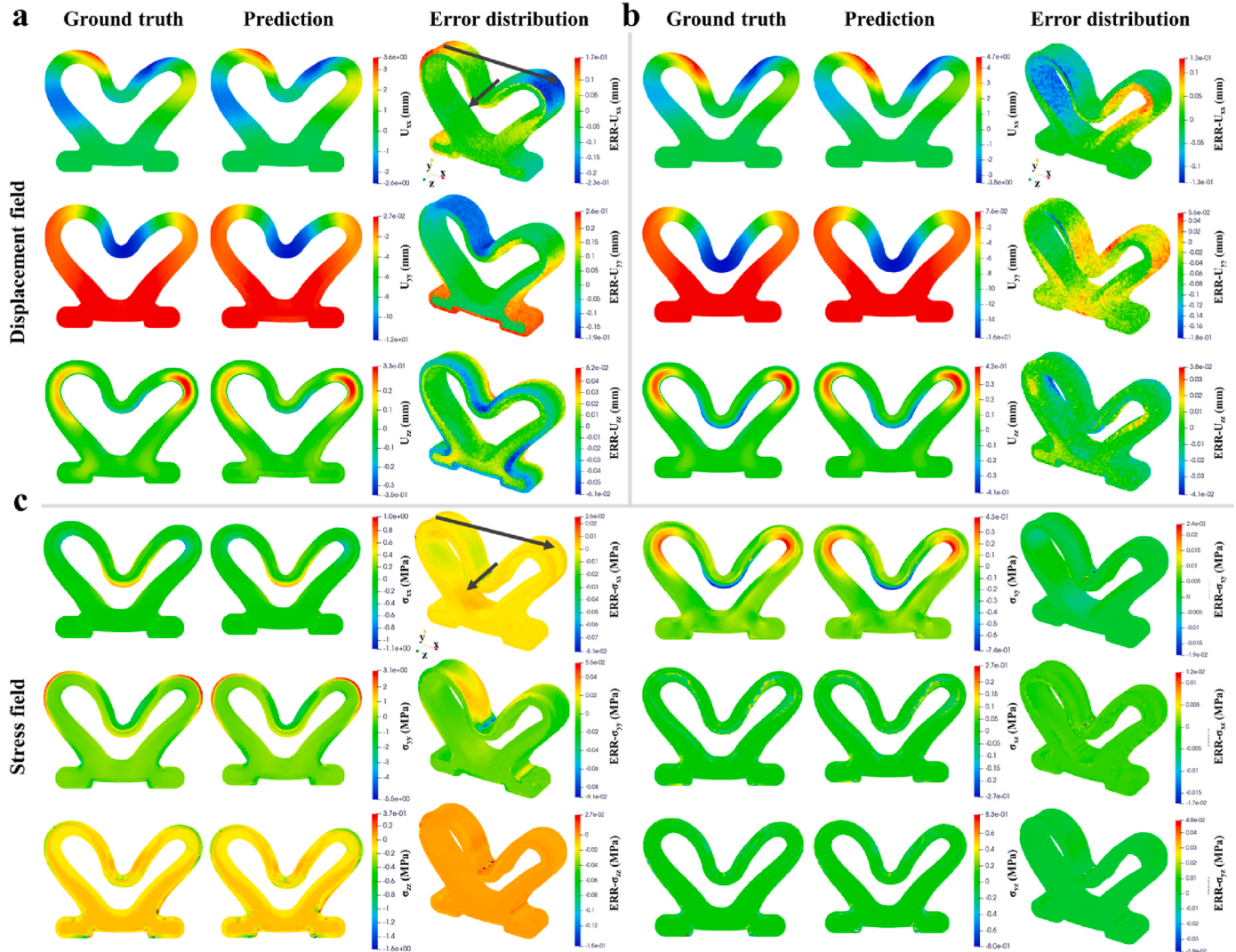


Fig. 4. Three examples of full-field displacement and stress predictions and error distributions: (a) H-DNNs displacement fields of 12.15 mm, pressure difference 35 kPa and 90 °C (NMAE = 0.80%, NAE-Peak = 1.67%). (b) H-DNNs displacement fields of 16.2 mm, pressure difference 20 kPa and 90 °C (NMAE = 0.22%, NAE-Peak = 0.93%). (c) H-DNNs stress fields of 16.2 mm, pressure difference 20 kPa and 90 °C (NMAE = 0.13%, NAE-Peak = 1.35%).

by supervised learning regression analysis with the mean square loss function, that is, the field codes are predicted from the input features, and then the field components are obtained by decoding. The Adam optimization algorithm [41] is used to update the training parameters. To evaluate the average predictive performance of the H-DNN architecture, the Monte Carlo cross-validation method is used as one of selectors with a sampling rate α within 50% and 80%, which means that the dataset is randomly split into two parts of D_{train} and $D_{validation}$ for training and validating the model, respectively. Validation and testing are performed using a standard desktop computer with an NVIDIA GeForce RTX 3090 GPU and Intel i9-9900K 3.60 GHz 16-core CPU.

The mean absolute error (MAE), normalized mean absolute error (NMAE), root mean square error (RMSE) and normalized absolute error of the peak value (NAE-Peak) are used as indicators to evaluate the global and local differences between actual values and predicted values. The MAE is defined as:

$$\text{MAE} = \frac{1}{N} \sum_{n=1}^N \|D_i^{(n)} - \hat{D}_i^{(n)}\| \quad (8)$$

The NMAE is defined as:

$$\text{NMAE} = \frac{\frac{1}{N} \sum_{n=1}^N \|D_i^{(n)} - \hat{D}_i^{(n)}\|}{\max\{D\} - \min\{D\}} \times 100\% \quad (9)$$

The RMSE is defined as:

$$\text{RMSE} = \sqrt{\frac{1}{N} \sum_{n=1}^N \|D_i^{(n)} - \hat{D}_i^{(n)}\|^2} \quad (10)$$

NAE-Peak is defined as:

$$\text{NAE-Peak} = \frac{\max(\|D_i^{(n)} - \hat{D}_i^{(n)}\|)}{\max\{D\} - \min\{D\}} \times 100\% \quad (11)$$

where n is the training data index and N is the size of training data related to the total number of nodes. The subscript i indicates the displacement and stress field component. When the prediction effect of the displacement/stress field is estimated as a whole, $D_i^{(n)}$ and $\hat{D}_i^{(n)}$ represent the displacement magnitude and the von Mises stress calculated by the FEM and DNNs, respectively. $\|\cdot\|$ means the absolute value. $\max\{D\}$ and $\min\{D\}$ represent the maximum and minimum values, respectively.

3. Results and discussion

3.1. Evaluation of the model performance

The effectiveness and the feasibility of surrogate models are verified by comparing the predicted displacement field and stress field results to the ground truth. Meanwhile, the experimental, simulated and predicted per unit length load-displacement curves at different temperatures are investigated to estimate the expansibility of the proposed method. Furthermore, the four representative error functions are selected to quantitatively evaluate the performance of surrogate models, and the optimal architecture is applied as the digital twin of the fabric rubber composite.

3.1.1. Full-field displacement and stress fields

As one surrogate model, the high-fidelity prediction ability and expandability of H-DNNs are explored by the regain of 3D full-field mechanical information. The predicted displacement and stress fields under different input conditions are illustrated qualitatively and quantitatively (see Figs. 4 and 5) by four error functions. The CCS exhibits

anisotropic nonlinear behaviours, and the NMAE and NAE-Peak of the displacement fields predicted by the H-DNNs are 0.54% and 1.86%, respectively, proving the acceptable deviation degree of peak values in the displacement field (see Fig. 5b). The prediction error distributions of the von Mises stress components demonstrate the excellent prediction performance of the H-DNNs (see Fig. 4 and Tables S9 and S10). The MAE, NMAE, RMSE and NAE-Peak of all predicted von Mises stress fields are 0.0065 MPa, 0.38%, 0.011 MPa and 4.51%, respectively, which reflects that the 3D stress fields obtained by H-DNNs show significantly smaller deviations than other machine learning architectures.

As shown in Fig. 4 and Supplementary Figs. 2–4, the prediction error distributions of the displacement and stress components predicted by H-DNNs are compared with those of the U-DNNs and D-DNNs, reflecting the high prediction accuracy of the H-DNNs. The prediction effect of the H-DNNs is better than that of the D-DNNs because the hierarchical prediction conforms to the multicomponent physical significance of composites and makes the predictor module more professional, which shows that the hierarchical predictor and automatic encoding-decoding module can improve the prediction accuracy of mechanical information.

Next, we examine the predicted accuracy of the H-DNNs for local-level displacement and stress components, and two representative prediction error distributions are selected and analysed, corresponding to the nodes involved by arrows along the x and z directions in Fig. 4. As shown in Fig. 5, the results show that H-DNNs provide reasonable prediction of 3D displacement and stress components, and the predicted results have regular consistency. The maximum absolute error of the displacement field is located in the small-deformation region subjected to displacement constraint conditions, as shown from Fig. 5a to c, which can be attributed to the approximately unchanged displacement of the constrained region under small deformation. The prediction accuracy of the stress field is much higher than that of the displacement field, as shown from Fig. 5d to e, which can be ascribed to the full-field stress distribution in the complex composite caused by any deformation. Therefore, the absolute error distribution of stress is mainly affected by the stress magnitude in each region. Moreover, it can be observed that H-DNNs can capture the true values well; even for some input conditions, there is a difference of 3 orders of magnitude between the displacement components (see Fig. 4b) and a difference of 4 orders of magnitude between the stress components (see Supplementary Fig. 4c). In principle, developing additional ML models for different mechanical prediction requirements could be improved, as the predicted fields in the H-DNNs could potentially serve as a valuable source for mechanical information.

3.1.2. Compression performance under different temperatures

In the second experiment, the accessibility and expandability of the H-DNNs is evaluated by extended tasks. For example, based on the environmental variables obtained from sensors and equilibrium conditions, the overall compression performance under different temperatures in the test dataset can be predicted by the H-DNNs from the summation of internal forces in all elements attached to nodes, which is compared with experimental and simulated data (see Fig. 6). The predicted results show good agreement with the experimental and simulated values. The maximum absolute error is 7.4% corresponding to the environment condition of 70 °C. In this case, the overall compression load acquired by the additional force sensor is used as a criterion to verify the H-DNN prediction, and the digital twin model can be calibrated using multiple sensors [10]. In addition, if the quantity measured by the sensor is considered as a controlling parameter, the number of input layer variables needs to be adjusted accordingly.

Furthermore, the exploration ability of the model for off-design space conditions is also examined. One of the loading displacements is

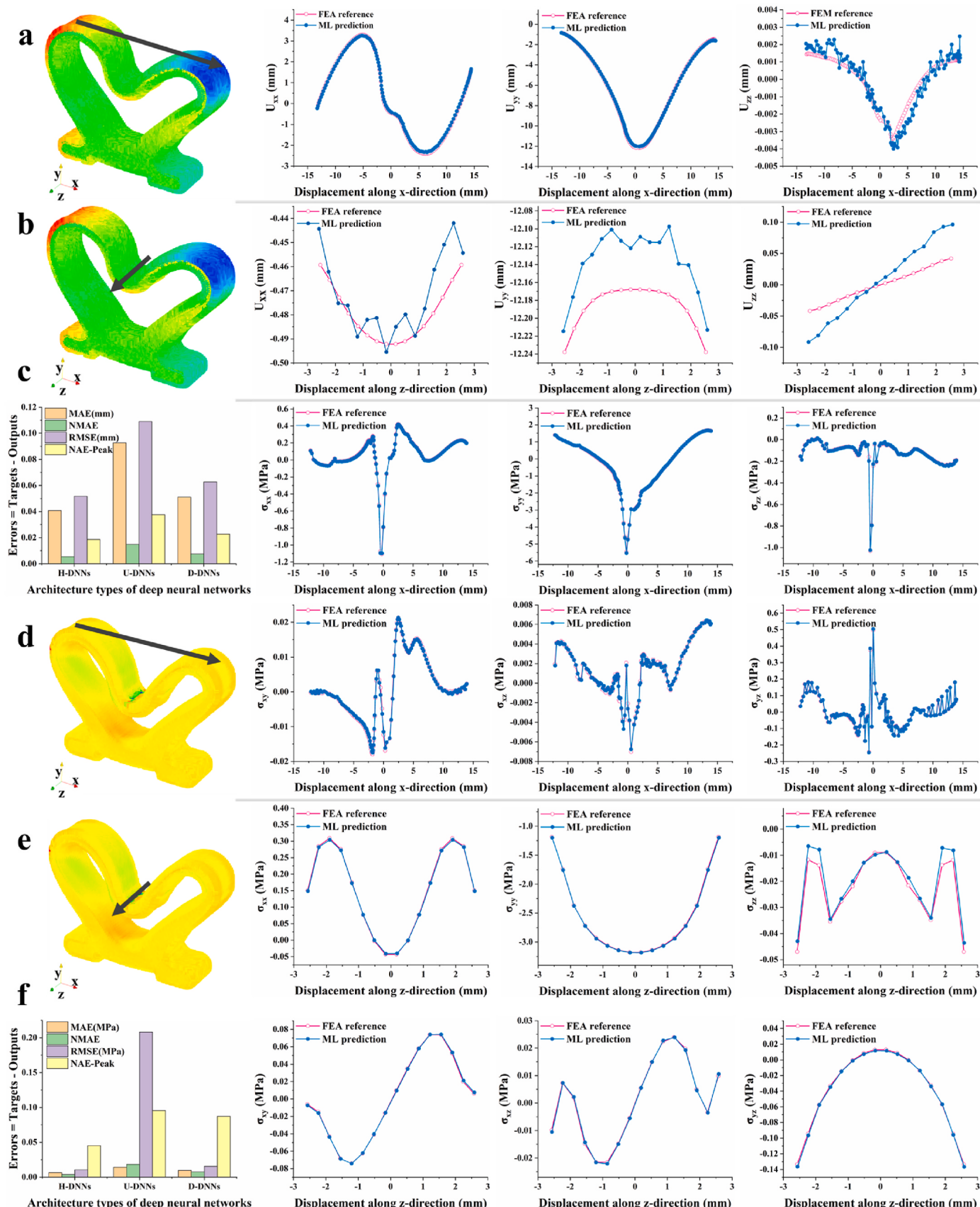


Fig. 5. Quantitative comparison of displacement and stress values: (a) The displacement components along the x direction. (b) The displacement components along the z direction. (c) Displacement fields prediction errors of three DNNs architectures. (d) The stress components along the x direction. (e) The stress components along the z direction. (f) Stress fields prediction errors of three DNNs architectures.

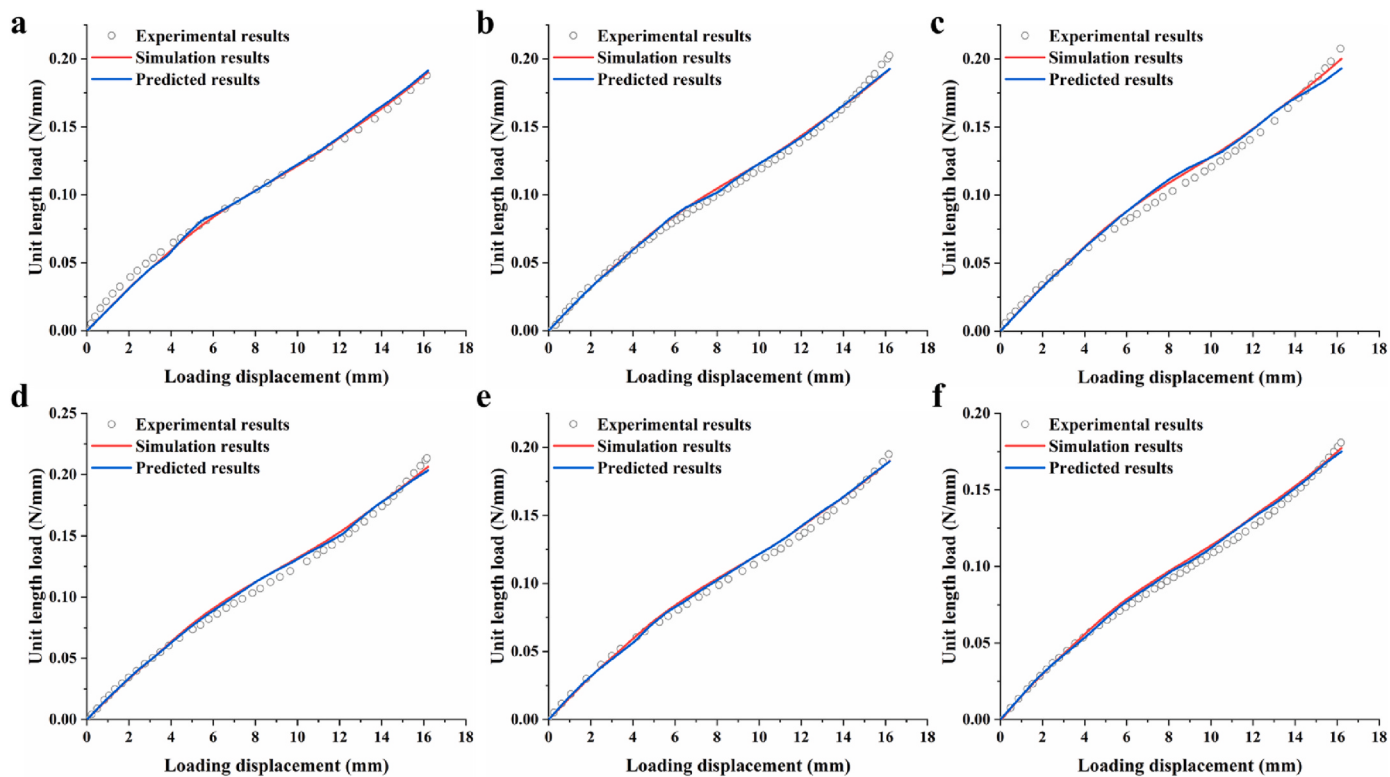


Fig. 6. Quantitative comparison of unsupervised overall prediction effect: (a-f) Comparisons among experimental, simulation and predicted compression performance at different temperatures of (a) 25 °C, (b) 50 °C, (c) 70 °C, (d) 90 °C, (e) 110 °C and (f) 130 °C.

set as 17.71 mm, exceeding the corresponding sampling boundary of 16.2 mm, and the other features are normally set as inputs. Surprisingly, the H-DNN model can still predict the displacement and stress fields accurately (see Supplementary Movie 1). These results suggest that the digital twin yields a degree of physical understanding of mechanical information for complex composites, which shows the potential of predicting multiple extended cases using the H-DNNs and provide evidence for transferability. In general, the H-DNNs show high accuracy and high-fidelity prediction of 3D displacement and stress components and overall compression performance, which is considered a compatible predictor.

Supplementary video related to this article can be found at <http://doi.org/10.1016/j.compscitech.2023.110139>

3.2. Case study of the digital twin

3.2.1. Real-time virtual-real interaction

In the third experiment, we demonstrate that H-DNNs digital twin could receive sensing data in real time, and present the operating results consistent with the physical entity, as well as abundant information. The interactive experiment between H-DNNs digital twin and physical entity is designed as shown in Fig. 7. The compression experiment of complex fabric rubber composite was carried out with a full loading displacement of 16.2 mm and a loading speed of 20 mm/min at room temperature and indoor pressure. An industrial surface array camera (Hikvision Digital Technology Co., MV-CH120-10UM/UC) is used to capture the deformation of the complex composite, and the digital image correlation (DIC) method is used to measure the displacement field under different loading displacements. The inputs are discrete data points collected by sensors. The pressure and temperature in the chamber, and loading

displacement of indenter are measured by one sensor, respectively. The stepper motor and the force sensor output the loading displacement and vertical load, respectively. The experimental conditions are collected and transmitted into the H-DNNs in real time, and H-DNNs performs the dynamic evolution of the digital twin at each acquisition frequency (frame), which realizes the synchronized comparison with DIC results (see Fig. 7a.).

The experimental displacement contours in x-y plane of the complex fabric rubber composite are shown in Fig. 7b. In this problem, it takes approximately 4 h to complete the FEM simulation using an 8-core computer server to obtain a set of field data results with the same input. The calculation time of DIC is approximately 5 min per frame at 2500 pixels s⁻¹. However, the H-DNNs digital twin performs predictions at the speed of millisecond level, and its corresponding computation time with the same computer configuration for three-dimensional full-field displacement and stress fields is about 10 ms. After synchronizing the time lines of the experimental and predicted data, four representative compressions are presented in Fig. 7b. The displacement fields reconstructed by H-DNNs are in agreements with the experimental results, and their maximum absolute errors are less than 5%, indicating the validity of the data generated by the H-DNNs digital twin.

Furthermore, taking the prediction and experiment results under a loading displacement of 11.93 mm as an example, the three-dimensional stress contours predicted by H-DNNs are shown in Fig. 7c, which illustrates that the digital twin can better realize synchronous and precise prediction of physical entities. While the high-precision reconstruction of 3D displacement and stress fields place more requirements on micro-CT equipment, demanding environments and complex algorithms, which means a longer time and an inability to provide direct information about the stress field. From this perspective, the digital twin

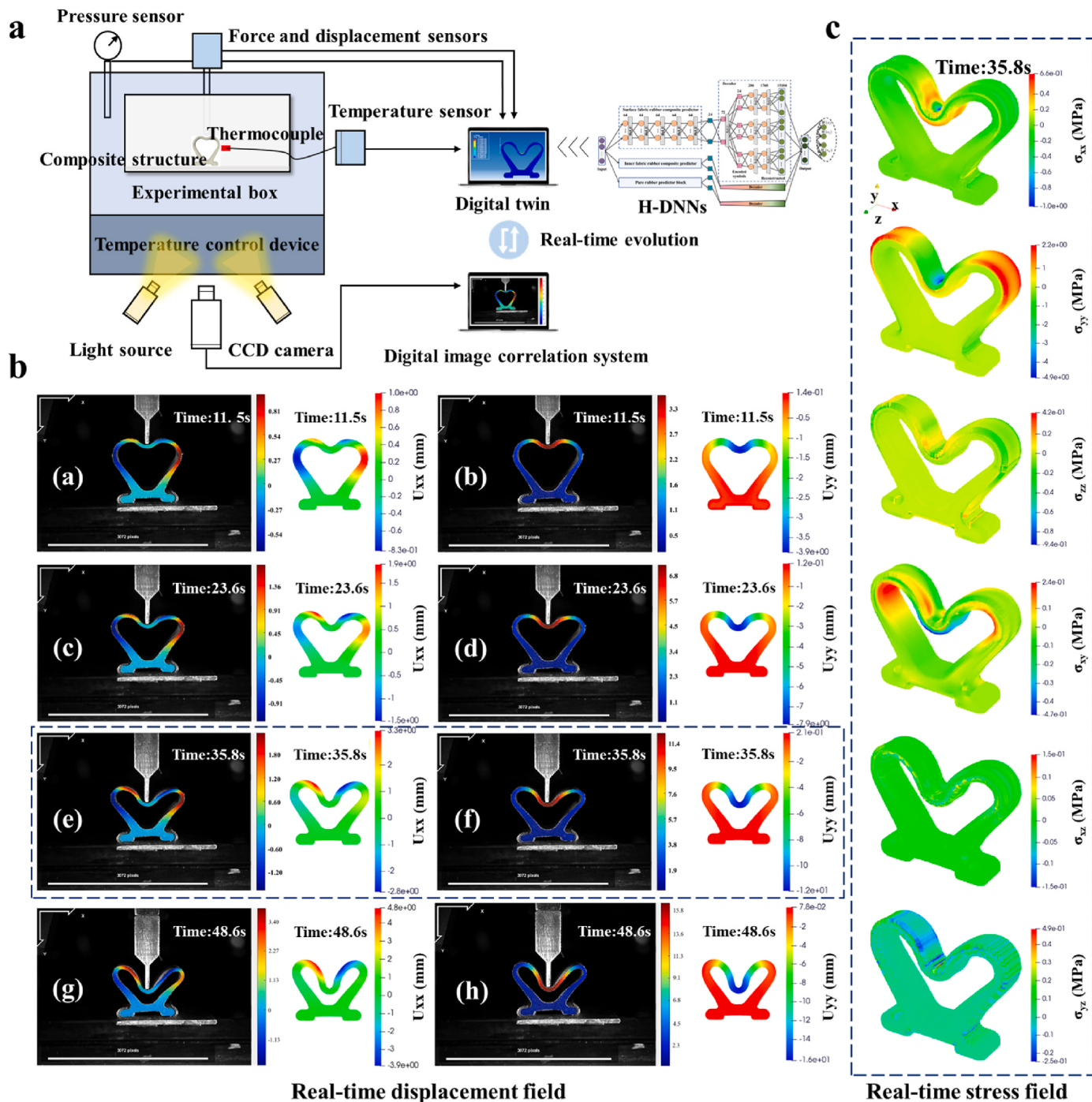


Fig. 7. Schematic diagram of digital twin interaction experiment and comparison of results: (a) A high and low temperature environment loading box with temperature, pressure, loading displacement and force sensors. Industrial cameras and light sources are used to calculate experimental displacement fields using digital image correlation methods. (b) Real time displacement fields of physical and H-DNNs digital twin. The displacement components and experimental time have been marked in the subfigure, corresponding to the loading displacements of 3.83 mm, 7.88 mm, 11.93 mm and 16.2 mm. (c) Real time three-dimensional full-field stress components predicted by H-DNNs digital twin under the loading displacement of 11.93 mm.

presents the high-fidelity real-time interaction with rich mechanical information of composites.

3.2.2. Performance prediction during cruising conditions

The benefits of the digital twin on the mechanical interaction are further investigated. The typical scenario of time-sensitive and knowledge-sensitive decision making is the state monitoring and control of aerospace components. The aircraft always encounters unpredictable disturbance of the external airflow and other influences during cruising

conditions, which generates complicated large deformation motion and vibration with a magnitude scale of mm . This change in loading displacement affects the sealing interface contact stress and flight safety [18]. The contact stress at any position can be monitored in real time by the digital twin. When the stresses in a certain area are less than the safe value (usually obtained by professional analysis), the load can be regulated by a feedback mechanism, which provides the possibility for intelligent control.

A virtual synchronous experiment is conducted to realize the real-

time process of "monitoring-feedback regulation". First, the monitoring data of loading displacement, temperature and pressure within 60 s in a disturbed phase are extracted during the whole cruising process (see Fig. 8a). The expected values of loading displacement, temperature, and low pressure are 16.2 mm, 30 °C and 75 kPa, respectively, which are accompanied by normally distributed random noise with 5% standard deviation (see Fig. 8b). Fluctuating environmental data as input features are substituted into the digital twin to predict the physical fields of the composite and the compression load obtained from the unsupervised process. One of the simplest regulatory mechanisms is that the compression within the next 2 s is specifically regulated to the expected value if the computed unit length load is less than its expected value. Two interaction modes with and without the self-regulating mechanism are set up. The overall unit length load on the whole composite and the

von Mises stresses of three representative nodes on its structure are predicted and analysed. Their mechanical information-time variation curves during cruising are illustrated in real time, as shown in Fig. 8c.

As shown in the red curve in Fig. 8c, the digital twin with regulatory feedback timely adjusts the composite seal structure according to the monitoring information and the specified mechanism, which maintains the target load and stress levels well. As a control, those of the composite without feedback adjustment (corresponding to without digital twin service) fluctuate with varying conditions, which may be potentially hazardous in practice. The time required for this application could be unacceptable if relying on conventional simulation analysis; for example, it takes approximately 240 h to calculate these full-field results of all frames by the FEM, which means that mobile computing cannot be achieved for such applications. The real-time mechanical evolution

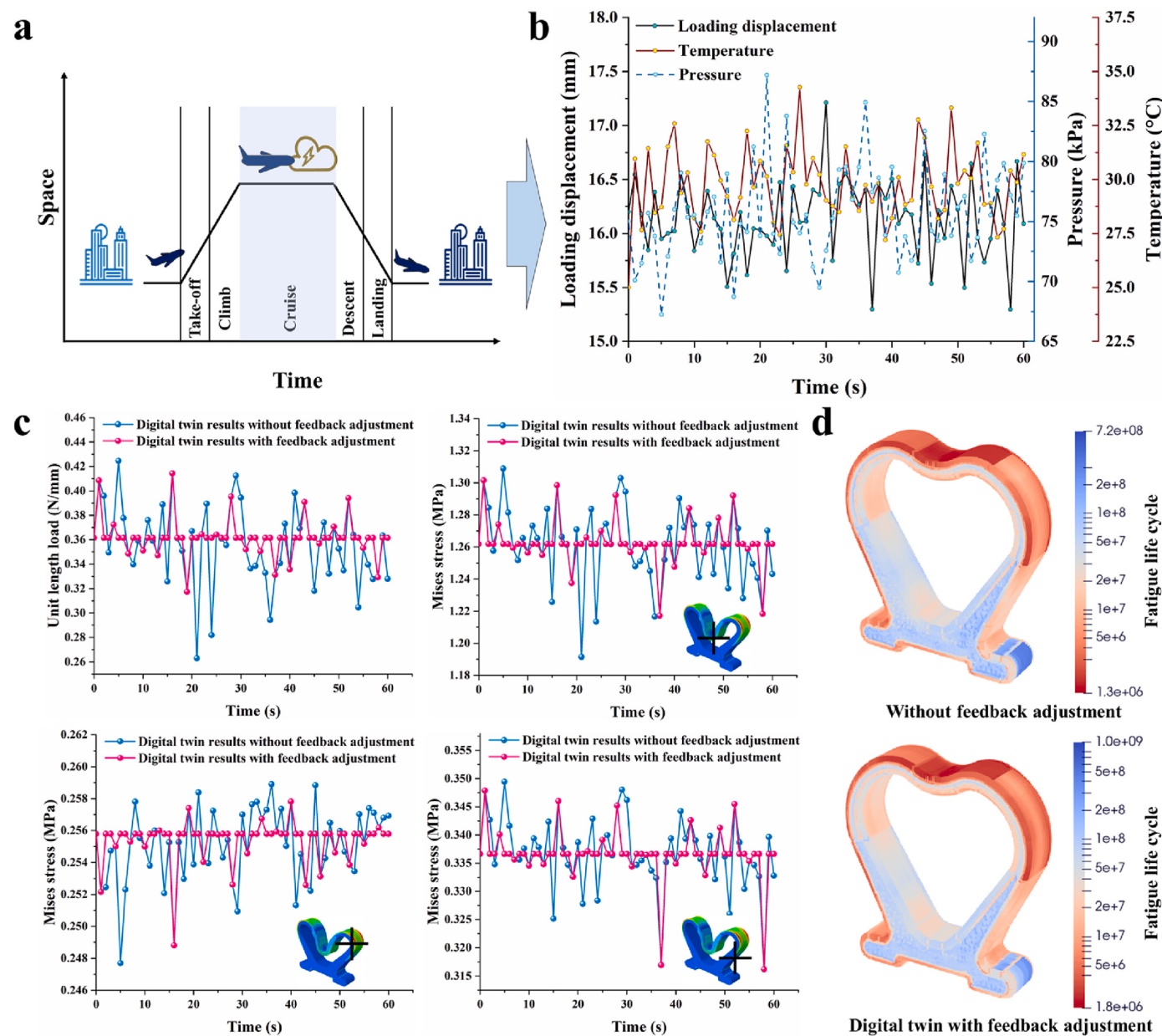


Fig. 8. Digital twin realizes model-data fusion and real-time life cycle assessment: (a) Flight status over time relative to space. The sudden alternating loads during the cruising condition are transmitted to the digital twin. (b) Simulated fluctuations of environmental data within 1 min. (c) Model-data fusion and feedback adjustment of composite digital twin. (d) Real-time fatigue life predictions by the digital twins without and with feedback adjustment.

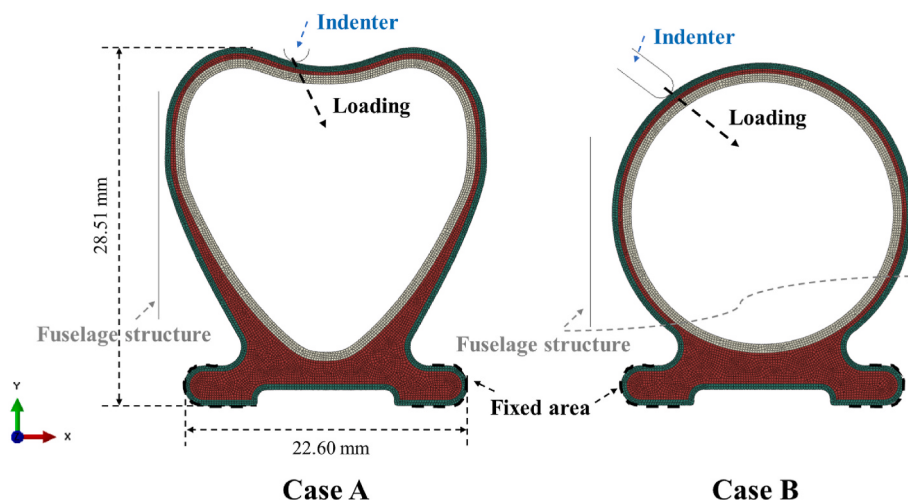


Fig. 9. Two examples of actual aircraft seal structures selected to produce datasets and the corresponding boundary conditions: (a) Case A with similar shapes and different materials, subjected to oblique loading displacement. (b) Case B with different shapes and different materials, subjected to oblique loading displacement.

ability of digital twin is fully demonstrated and shows rich intelligent application potential.

3.2.3. Fatigue lifetime assessment under service status

Lifetime management of composites in real applications in which the composites are exposed to complicated time-domain cycles has become essential issues facing investigators, which is one of the considerable number of advantages of composite digital twin. The improved online rain-flow algorithm [42] enables interaction between the waveform sorted by damage during a given complicated loading, it hence is used to evaluate the effective waveform of fatigue life under complicated loading, as shown in [Supplementary Fig. 5](#). Considering a modified Smith-Watson-Topper (SWAT) model [43], the expected life and cumulative damage caused by complicated loads can be obtained based on the Miner cumulative damage law [44] and the real-time data generated by the digital twin, and the accumulated fatigue damage by the i-th harmonic strain cycle could be expressed as [43]:

$$\bar{D}_i = \frac{n_i}{(N_f)_i} = 2n_i \left(\frac{K_f \sigma_a \sqrt{1 + \sigma_m/\sigma_a}}{\sigma_{\max} \epsilon_a} \right)^{1/b} \quad (12)$$

where σ_{\max} , σ_m and σ_a are the maximum stress, stress amplitude and mean stress of each distinct cycle calculated by the four-point rain-flow counting algorithm, respectively; ϵ_a is the corresponding strain amplitude; n_i is the number of stress-strain hysteresis loops; K_f and b are the material parameters that are set as 30.7003 and -0.8754, respectively, estimated from the fatigue tests [43].

The digital twins allow real-time prediction of composite behaviours, and for online life assessment of a given sampling interval, the steps can be decomposed into the following steps: (i) By utilizing the H-DNNs, the von Mises stress-time histories are calculated node by node for the complex composite within the given inputs (taking 60 s as an example, see [Fig. 8b](#)). (ii) We take a stress-time history curve over time as the abscissa and stress as the ordinate and rotate the curve 90° clockwise. The lines between data points are similar to rows of roofing layers, and data recording points are similar to rows of raindrops. The process of statistics is as follows: rain drops in turn along the inner side of the roof of different layers down to the bottom. The total number of cycles N_s and the number of repeats n are obtained. (iii) The accumulated fatigue damage \bar{D} in a single deformation period is calculated by the Miner cumulative damage law [44]. (iv) Life prediction and real-time decision making of composite materials are enabled. The calculation details and data are summarized in [Supplementary Note 1](#).

[Fig. 8d](#) shows the predicted lifetime of the digital twin subjected to

the loading history in [Fig. 8b](#). The minimum life cycle of the composite without feedback regulation occurs in the surface dense fabric rubber layer with 1.3×10^6 cycles, which is close to the actual order of magnitude. The complex composite presents an asymmetric fatigue life-cycle contour due to the difference between internal pressure and external pressure and not strictly symmetrical shapes. Additionally, the composite digital twin with feedback regulation mechanisms shows great potential for improving the life of composites (1.8×10^6 cycles), which demonstrates the ability of composite digital twins to predict and improve the fatigue life. It should be noted that this section focuses on demonstrating the ability of composite digital twins to predict fatigue life and does not strictly consider the relationship of multistage loading order, which does not prevent the possibility of a more refined assessment.

3.3. Applicability and extrapolation

In this section, two examples of actual aircraft seal structures are selected to produce datasets for illustrating the applicability of the present method to composite components with different shapes/designs and made of different materials. These two 1.0-mm-thick structures are of the same material type themselves, but have different constitutive models from the seal structure shown in [Fig. 1c](#). The engineering constants model of the surface fabric rubber composite adopts different homogenized anisotropic parameters. The constitutive model of the inner fabric rubber composite is selected from Ref. [45], and the Neo-Hookean strain-energy function is applied to the pure rubber layer [36]. The detailed parameters are shown in [Table S11](#). In addition, case A adopts a similar shape, which is equivalent to a major change in the loading form; In case B, different shapes and more complex loading forms and boundary conditions are adopted. Regardless of internal and external pressures, the inputs to the model are temperature T and the loading displacement d_x and d_y in both directions. As shown in [Fig. 9](#), the final absolute loading displacement along the x and y directions are 2.5 mm and -7.9 mm (case A), 7.33 mm and -5.23 mm (case B), respectively. Following the steps in Section 2.4, 97 and 104 samples are generated for case A and Case B, respectively, within the temperature range and within the loading displacement in the loading direction described above. After changing the input to temperature and loading displacements, both case A and case B are trained with the same H-DNNs architecture shown in [Fig. 2](#).

The predictive effects of the H-DNNs architecture on case A and case B are shown in [Fig. 10](#). The MAE and NMAE of predicted results in case A and case B are 0.076 MPa, 5.1% and 0.038 MPa, 4.6%, respectively. It



Fig. 10. Prediction results and error distributions of stress fields for case A and case B. (a) Case A at 0 °C, 4.12 mm and 2.95 mm as inputs. (b) Case B at -30 °C, 1.22 mm and 3.86 mm as inputs.

can be seen that the predicted results of the stress components are in good agreement with the ground truth. At the same time, the prediction error of the stress component along the tangential direction is slightly larger than that in the main direction, and improving the training weight of each region according to the demand is an optional method. In general, these results illustrate that the H-DNNs architecture can be applicable to different shapes/designs and different materials.

Furthermore, the extrapolation capabilities of the H-DNNs architecture are explored by 4 selected cases: (i) keep 25 °C and 16.2 mm loading displacement, and change the external pressure from 52 kPa to 42 kPa; (ii), (iii) and (iv) keep the external pressure at 102 kPa and change the loading displacement from 16.2 mm to 17.0 mm at 25, 70 and 130 °C. Under the above conditions, the prediction ability of H-DNNs model outside the design space was evaluated by taking the prediction of the inner fabric rubber layer with the most complex constitutive relationship as an example. The four error functions given in Section 2.5 are used to evaluate the extrapolation ability of the model, and the results are shown in Fig. 11. Fig. 11a shows the FEM truth values

corresponding to 52 kPa and 42 kPa of external pressure, and it can be seen that pressure affects the stress state of the given CCS. The model has a good extrapolation capability, with acceptable accuracy even at 42 kPa. These results further demonstrate the extrapolation capability and applicability of H-DNNs.

As shown in Fig. 11b, for 25, 70 and 130 °C, when the loading displacement exceeds the training upper bound of 16.2 mm, the predicted results are still consistent with the FEM truth value and gradually diverge. In addition, the error values of different temperatures have stronger nonlinearity, which may be attributed to the significant effect of temperature on the nonlinear constitutive behavior of internal fabric rubber composites. It can be seen that the input control parameters that affect the nonlinear behavior of CCS are related to the prediction effect of the neural network.

3.4. Transfer learning

The transfer learning ability is explored to efficiently assist in the

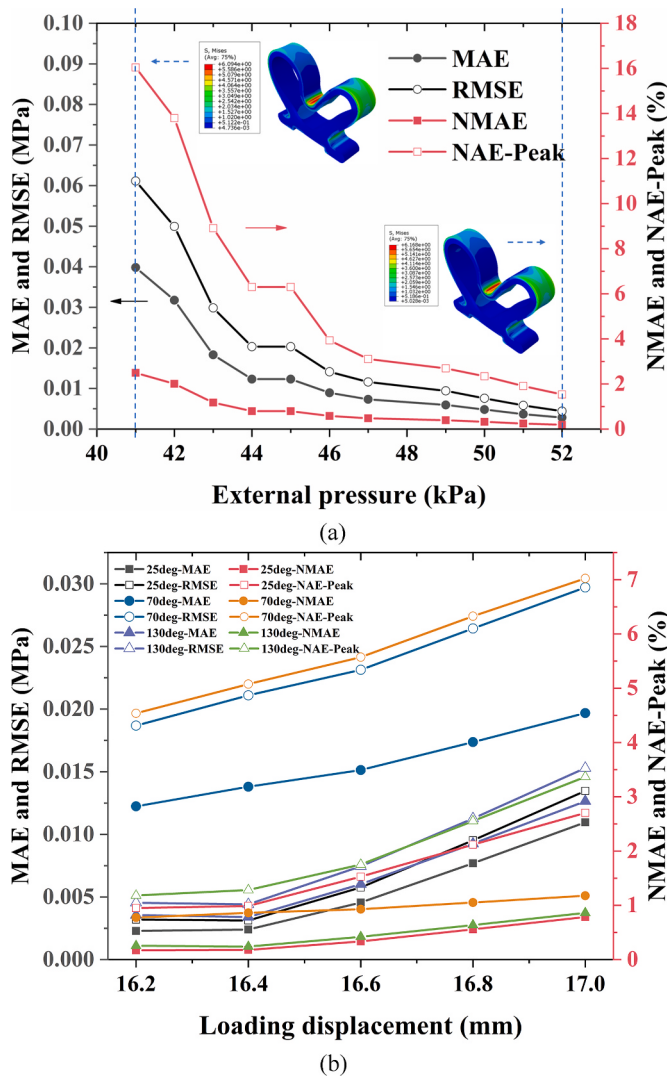


Fig. 11. Exploration of the extrapolation capability of H-DNNs architecture. (a) Only the external pressure is changed below the training lower bound of 52 kPa for 25 °C, 16.2 mm loading displacement. (b) Keep the external pressure at 102 kPa and change the loading displacement beyond the training upper bound of 16.2 mm for 25, 70 and 130 °C.

automatic evaluation of composites. We use pretrained H-DNNs and untrained H-DNNs to retrain in a temperature range different from that in Table S8. As shown in Fig. 12, the transfer learning with pretrained parameters demonstrates a faster overall training time, approximately five times quicker than the alternative. Additionally, it exhibits improved slope and asymptotic behavior during training. These results demonstrate that the trained model captures the constitutive behaviour of similar composites and produces good generalization performance on related tasks. After the first training, other composite digital twins can be quickly identified by transfer learning.

Collectively, these findings provide the possibility for the cost-effective and refined development of digital twin infrastructures. Many opportunities exist, such as the introduction of shape coding and image learning algorithms, to develop digital twins of various shapes that will expand the ability to the manufacturing, analysis, and optimization of composites in high throughput. More physical models are the driving factor determining the performance of digital twins. In addition, the number of sensors can be increased to achieve more digital twinning functions. Changing the sampling methods, such as selecting the Stratified K-Fold Cross-Validation [46], can be one way to improve the presented method which deserves to be investigated in further work.

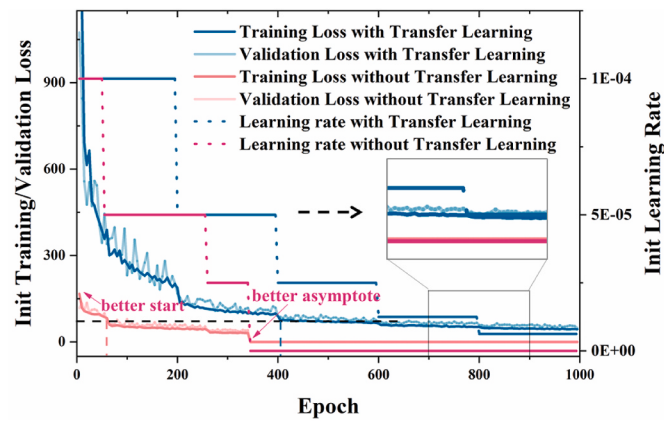


Fig. 12. Effect of the transfer learning method on computational efficiency and accuracy of the H-DNN digital twins.

4. Conclusions

In this work, the feasibility of DL-based realization of complex composite twins for complex fabric rubber composite are systematically developed. The effectiveness of the proposed method is verified by representative case studies. Some important conclusions are summarized as:

- (1) The general framework of composite digital twin and its full-field mechanical components prediction are presented. Digital twins can be constructed based on experimental observations, expert knowledge, machine learning methods and sensor transmission devices. The model of complex fabric rubber composite based on FEM can provide clean and effective training data for the generation of digital twins.
- (2) Three types of networks are proposed as surrogate models for three-dimensional displacement and stress fields of complex fabric rubber composites, also the prediction effect and calculation accuracy of different surrogate models are evaluated with both quantitative and qualitative error assessments, which proves the feasibility and stability for predicting large-scale variables from control parameters. Hierarchical calculation and autoencoder have great potential in dealing with complex displacement and stress fields of composites.
- (3) The real-time interactive verification experiments are conducted to demonstrate the high-fidelity real-time computing capability of digital twin. The digital twin performs predictions at the speed of millisecond level, and the average normalized mean absolute errors of displacement and stress fields are 0.54% and 0.38%, respectively. Compared with the accuracy and efficiency of traditional methods, digital twin exhibits excellent simulated and predicted performance. Representative cases demonstrate that H-DNNs architecture can be generalized to other design/shape and materials, and has potential extrapolation capabilities.
- (4) A simple and clear "monitoring-feedback-regulation" case is given, and a virtual experiment is carried out to realize the real-time process. We observed that digital twin enables material-dependent data to synchronize with timeline for dynamic processes and decision-making. The realization of model-data fusion may make investigators pay attention to the feasibility and great potential between deep learning and digital twin. It is expected that more digital twins may be accumulated which show strategic implications in virtual-reality interaction, high-throughput computing, multi-field coupling, life assessment, intelligent control and other fields in the future.

CRediT authorship contribution statement

X.F.Y conceptualized the idea, and guided and supervised the research. X.Y.X enriched the methodology, generated, gathered and analysed the learning data, led the mechanics modeling, software designs and experimental work, with assistance from G.W.W. X.F.Y and X.Y.X wrote the manuscript and designed figures. H.Y and L.B.Z read and edited the manuscript. All authors commented on the paper.

Declaration of competing interest

The authors declare that they have no known competing financial interests or personal relationships that could have appeared to influence the work reported in this paper.

Data availability

Data will be made available on request.

Acknowledgements

This work was supported by the National Natural Science Foundation of China (Grant Nos. 12172191).

Appendix A. Supplementary data

Supplementary data to this article can be found online at <https://doi.org/10.1016/j.compscitech.2023.110139>.

References

- [1] A. Morch, L. Astruc, J.F. Witz, F. Lesaffre, P. Lecomte-Grosbras, D. Soulard, M. Brieu, Modeling of anisotropic hyperelastic heterogeneous knitted fabric reinforced composites, *J. Mech. Phys. Solid.* 127 (2019) 47–61, <https://doi.org/10.1016/j.jmps.2019.03.006>.
- [2] X. Xu, G. Wang, H. Yan, X. Yao, Constitutive relationship of fabric rubber composites and its application, *Compos. Struct.* 304 (2023), 116302, <https://doi.org/10.1016/j.compsctruct.2022.116302>.
- [3] M.A. Ali, Q. Guan, R. Umer, W.J. Cantwell, T. Zhang, Efficient processing of µCT images using deep learning tools for generating digital material twins of woven fabrics, *Compos. Sci. Technol.* (2022), <https://doi.org/10.1016/j.compscitech.2021.109091>.
- [4] F. Tao, Q. Qi, L. Wang, A.Y.C. Nee, Digital twins and cyber-physical systems toward smart manufacturing and Industry 4.0: correlation and comparison, *Engineering* (2019), <https://doi.org/10.1016/j.eng.2019.01.014>.
- [5] Fei Tao, Qinglin Qi, Make more digital twins, *Nature* 573 (2019) 490–491, <https://doi.org/10.1038/d41586-019-02849-1>.
- [6] E.H. Glaessgen, D.S. Stargel, The digital twin paradigm for future NASA and U.S. Air force vehicles, in: *Collect. Tech. Pap. - AIAA/ASME/ASCE/AHS/ASC Struct. Struct. Dyn. Mater. Conf.*, 2012, <https://doi.org/10.2514/6.2012-1818>.
- [7] AIAA, *Digital Twin : Definition & Value*, 2020.
- [8] Y. Lu, C. Liu, K.I.K. Wang, H. Huang, X. Xu, Digital Twin-driven smart manufacturing: connotation, reference model, applications and research issues, *Robot. Comput. Integrated Manuf.* (2020), <https://doi.org/10.1016/j.rcim.2019.101837>.
- [9] P. Bauer, P.D. Dueben, T. Hoefer, T. Quintino, T.C. Schulthess, N.P. Wedi, The digital revolution of Earth-system science, *Nat. Comput. Sci.* 1 (2021) 104–113, <https://doi.org/10.1038/s43588-021-00023-0>.
- [10] M.G. Kapteyn, J.V.R. Pretorius, K.E. Willcox, A probabilistic graphical model foundation for enabling predictive digital twins at scale, *Nat. Comput. Sci.* 1 (2021) 337–347, <https://doi.org/10.1038/s43588-021-00069-0>.
- [11] R. Laubenbacher, J.P. Sluka, J.A. Glazier, Using digital twins in viral infection, *Science* 80 (2021), <https://doi.org/10.1126/science.abf3370>.
- [12] M. Liu, S. Fang, H. Dong, C. Xu, Review of digital twin about concepts, technologies, and industrial applications, *J. Manuf. Syst.* (2021), <https://doi.org/10.1016/j.jmsy.2020.06.017>.
- [13] B. Wang, G. Zhang, H. Wang, J. Xuan, K. Jiao, Multi-physics-resolved digital twin of proton exchange membrane fuel cells with a data-driven surrogate model, *Energy AI* (2020), <https://doi.org/10.1016/j.egyai.2020.100004>.
- [14] F. Bai, H.B. Quan, R.J. Yin, Z. Zhang, S.Q. Jin, P. He, Y.T. Mu, X.M. Gong, W. Q. Tao, Three-dimensional multi-field digital twin technology for proton exchange membrane fuel cells, *Appl. Energy* 324 (2022), <https://doi.org/10.1016/j.apenergy.2022.119763>.
- [15] M. Wang, S. Feng, A. Incecik, G. Królczyk, Z. Li, Structural fatigue life prediction considering model uncertainties through a novel digital twin-driven approach, *Comput. Methods Appl. Mech. Eng.* 391 (2022), 114512, <https://doi.org/10.1016/j.cma.2021.114512>.
- [16] G. Seon, Y. Nikishkov, A. Makeev, L. Ferguson, Towards a digital twin for mitigating void formation during debulking of autoclave composite parts, *Eng. Fract. Mech.* (2020), <https://doi.org/10.1016/j.engfracmech.2019.106792>.
- [17] Q. Wang, W. Jiao, Y.M. Zhang, Deep learning-empowered digital twin for visualized weld joint growth monitoring and penetration control, *J. Manuf. Syst.* (2020), <https://doi.org/10.1016/j.jmsy.2020.10.002>.
- [18] H. Yang, W.F. Wang, J.C. Shang, P.D. Wang, H. Lei, H. sen Chen, D.N. Fang, Segmentation of computed tomography images and high-precision reconstruction of rubber composite structure based on deep learning, *Compos. Sci. Technol.* 213 (2021), 108875, <https://doi.org/10.1016/j.compscitech.2021.108875>.
- [19] V. Sadrmansh, Y. Chen, Simulation of tensile behavior of plant fibers using the Discrete Element Method (DEM), *Compos. Part A Appl. Sci. Manuf.* (2018), <https://doi.org/10.1016/j.compositesa.2018.08.023>.
- [20] L. Yuan, X. Yao, H. Yang, Multiscale modelling of strain-resistance behaviour for graphene rubber composites under large deformation, *Nanoscale* (2019), <https://doi.org/10.1039/c9nr05036a>.
- [21] D. Marinovic, M. Zehn, Survey of finite element method-based real-time simulations, *Appl. Sci.* (2019), <https://doi.org/10.3390/app9142775>.
- [22] M.C. Kennedy, A. O'Hagan, Bayesian calibration of computer models, *J. R. Stat. Soc. Ser. B Stat. Methodol.* (2001), <https://doi.org/10.1111/1467-9868.00294>.
- [23] C. Bonatti, D. Mohr, One for all: universal material model based on minimal state-space neural networks, *Sci. Adv.* (2021), <https://doi.org/10.1126/sciadv.abf3658>.
- [24] M. Flaschel, S. Kumar, L. De Lorenzis, Unsupervised discovery of interpretable hyperelastic constitutive laws, *Comput. Methods Appl. Mech. Eng.* (2021), <https://doi.org/10.1016/j.cma.2021.113852>.
- [25] M. Mozaffar, R. Bostanabad, W. Chen, K. Ehmann, J. Cao, M.A. Bessa, Deep learning predicts path-dependent plasticity, *Proc. Natl. Acad. Sci. U.S.A.* (2019), <https://doi.org/10.1073/pnas.1911815116>.
- [26] Z. Yang, C.H. Yu, M.J. Buehler, Deep learning model to predict complex stress and strain fields in hierarchical composites, *Sci. Adv.* (2021), <https://doi.org/10.1126/SCIADEV.ABD7416>.
- [27] Z. Yang, C.H. Yu, K. Guo, M.J. Buehler, End-to-end deep learning method to predict complete strain and stress tensors for complex hierarchical composite microstructures, *J. Mech. Phys. Solid.* (2021), <https://doi.org/10.1016/j.jmps.2021.104506>.
- [28] Z. Liu, C.T. Wu, Exploring the 3D architectures of deep material network in data-driven multiscale mechanics, *J. Mech. Phys. Solid.* (2019), <https://doi.org/10.1016/j.jmps.2019.03.004>.
- [29] S. Fan, J. Zhang, B. Wang, J. Chen, W. Yang, W. Liu, Y. Li, A deep learning method for fast predicting curing process-induced deformation of aeronautical composite structures, *Compos. Sci. Technol.* 232 (2023), 109844, <https://doi.org/10.1016/j.compscitech.2022.109844>.
- [30] G.R. Liu, A step-by-step method of rule-of-mixture of fiber- and particle-reinforced composite materials, *Compos. Struct.* (1997), [https://doi.org/10.1016/S0263-8223\(98\)00033-6](https://doi.org/10.1016/S0263-8223(98)00033-6).
- [31] D.P. Kingma, M. Welling, Auto-encoding variational bayes, *Conf. Track Proc.* (2014), <https://doi.org/10.48550/arXiv.1312.6114>.
- [32] Y. Huang, W. Jin, Z. Yu, B. Li, Supervised Feature Selection through Deep Neural Networks with Pairwise Connected Structure, *Knowledge-Based Syst.*, 2020, <https://doi.org/10.1016/j.knosys.2020.106202>.
- [33] Y. Dong, X. Yao, H. Yan, L. Yuan, H. Yang, Macro- and mesoscopic mechanical properties of complex fabric rubber composite under different temperatures, *Compos. Struct.* (2019), <https://doi.org/10.1016/j.compsctruct.2019.111510>.
- [34] H. Yang, L. Yuan, X.F. Yao, D.N. Fang, Piezoresistive response of graphene rubber composites considering the tunneling effect, *J. Mech. Phys. Solid.* (2020), <https://doi.org/10.1016/j.jmps.2020.103943>.
- [35] M. Mooney, A theory of large elastic deformation, *J. Appl. Phys.* 11 (1940) 582–592, <https://doi.org/10.1063/1.1712836>.
- [36] R.S. Rivlin, P. Trans, R.S. Lond, Large elastic deformations of isotropic materials IV. further developments of the general theory, *Philos. Trans. R. Soc. London. Ser. A, Math. Phys. Sci.* 241 (1948) 379–397, <https://doi.org/10.1098/rsta.1948.0024>.
- [37] X. Xu, H. Yan, C. Xiao, X. Yao, An anisotropic hyper-visco-pseudo-elastic model and explicit stress solutions for fabric reinforced rubber composites, *Int. J. Solid Struct.* 242 (2022), 111519, <https://doi.org/10.1016/j.ijisolstr.2022.111519>.
- [38] X. Xu, X. Yao, Y. Dong, H. Yang, H. Yan, Mechanical behaviors of non-orthogonal fabric rubber seal, *Compos. Struct.* (2021), <https://doi.org/10.1016/j.compsctruct.2020.113453>.
- [39] Y. Wang, F. Tao, Y. Zuo, M. Zhang, Q. Qi, Digital-twin-enhanced quality prediction for the composite materials, *Engineering* (2023), <https://doi.org/10.1016/j.eng.2022.08.019>.
- [40] H. Ziaeipoor, M. Taylor, M. Pandey, S. Martelli, A novel training-free method for real-time prediction of femoral strain, *J. Biomech.* (2019), <https://doi.org/10.1016/j.jbiomech.2019.01.057>.
- [41] D.P. Kingma, J.L. Ba, Adam: a method for stochastic optimization, in: *3rd Int. Conf. Learn. Represent. ICLR 2015 - Conf. Track Proc.*, 2015.
- [42] V. Samavatian, H. Iman-Eini, Y. Avenas, An efficient online time-temperature-dependent creep-fatigue rainflow counting algorithm, *Int. J. Fatig.* (2018), <https://doi.org/10.1016/j.ijfatigue.2018.06.037>.

- [43] J.R. Cho, Y.H. Yoon, C.W. Seo, Y.G. Kim, Fatigue life assessment of fabric braided composite rubber hose in complicated large deformation cyclic motion, *Finite Elem. Anal. Des.* 100 (2015) 65–76, <https://doi.org/10.1016/j.finel.2015.03.002>.
- [44] M. Kawai, Y. Ishizuka, Fatigue life of woven fabric carbon/epoxy laminates under alternating R-ratio loading along non-proportional path in the σ_m - σ_a plane, *Int. J. Fatig.* (2018), <https://doi.org/10.1016/j.ijfatigue.2018.02.036>.
- [45] H. Yang, X.F. Yao, Y.C. Ke, Y. ji Ma, Y.H. Liu, Constitutive behaviors and mechanical characterizations of fabric reinforced rubber composites, *Compos. Struct.* 152 (2016) 117–123, <https://doi.org/10.1016/j.compstruct.2016.05.021>.
- [46] S. Yadav, S. Shukla, Analysis of K-Fold Cross-Validation over hold-out validation on colossal datasets for quality classification, in: Proc. - 6th Int. Adv. Comput. Conf, IACC 2016, 2016, <https://doi.org/10.1109/IACC.2016.25>.